



Coupled reaction mechanism reduction for the hetero-/homogeneous combustion of syngas over platinum

Ran Sui^{a,*}, Wenkai Liang^a, John Mantzaras^b, Chung K. Law^{a,c}

^a Department of Mechanical and Aerospace Engineering, Princeton University, Princeton, NJ 08544, USA

^b Laboratory for Scientific Computing and Modeling, Paul Scherrer Institute, Villigen PSI CH-5232, Switzerland

^c Center for Combustion Energy, Tsinghua University, Beijing 100084, China



ARTICLE INFO

Article history:

Received 3 June 2019

Revised 16 October 2019

Accepted 9 December 2019

Keywords:

Mechanism reduction

Hetero-/homogeneous combustion

Directed relation graph (DRG)-based method, H₂/CO oxidation over Pt

ABSTRACT

Coupled reduced mechanisms were developed for the hetero-/homogeneous combustion of fuel-lean and fuel-rich H₂/CO/O₂/N₂ mixtures in a Pt-coated planar channel, using a method based on the Directed Relation Graph (DRG) and for a wide range of operating conditions for which detailed measurements are available. It is demonstrated that catalytic and gas-phase reaction mechanisms can be reduced together for all the fuel-lean cases. On the other hand, when joint reduction is performed for low-pressure fuel-rich cases (using a strict threshold value to capture the relatively weak, yet still important coupling between the catalytic and gas-phase reaction pathways) the result is a less efficient reduction process. For the high-pressure fuel-rich cases the catalytic-gaseous chemical coupling is weak enough to be neglected such that the reduction can be conducted separately for higher reduction efficiency. The reduced mechanisms reproduced well the major gaseous species concentrations, gas temperatures and homogeneous ignition distances obtained with the detailed mechanisms, thus demonstrating the capacity of the applied method in reducing catalytic/gas-phase reaction mechanisms. In addition, it is shown that for fuel-lean stoichiometries the reduction could provide a rapid indication if gas-phase combustion is ignited, without the need of full simulations. The reduced mechanisms are expected to facilitate large-scale simulations, with fidelity, for the design and thermal management of practical catalytic combustion systems.

© 2019 The Combustion Institute. Published by Elsevier Inc. All rights reserved.

1. Introduction

Catalytic processes in turbulent flows are of relevance in gas turbines of power generation systems [1, 2], automotive exhaust gas converters [3], and reactors for the synthesis of high-value chemicals from hydrocarbon feedstocks [4]. In gas turbines, the high inlet Reynolds numbers (up to ~20,000 based on the individual catalytic channel hydraulic diameter [5]) warrant turbulent flows. On the other hand, transition to turbulence by means of geometrical modifiers enhances transport and can increase the automotive catalytic converter efficiency by up to ~30% [6,7]. Furthermore, catalytic fuel processing typically proceeds first via fuel reforming to syngas and then by the Fisher-Tropsch (F-T) synthesis of the desired chemical; the trend nowadays is to carry out the entire process at high pressures (up to 50 bar) dictated by the downstream F-T, and such elevated pressures typically lead to turbulent flows.

Turbulent flows in catalytic combustion systems hinder the inclusion of detailed chemistry in large-scale numerical investigations due to the excessive computational costs. For this reason, previous 3-D large eddy simulations (LES) [8,9] and direct numerical simulations (DNS) [10,11] have mainly adopted one-step catalytic reaction mechanisms without gas-phase chemistry. Only very recently, detailed catalytic and gas-phase chemistries have been applied in a 3-D DNS study of H₂/air combustion in a Pt-coated planar channel [12], at inlet Reynolds numbers (based on the 5 mm channel height) up to 12,360. Recognizing the need to be computationally feasible while still chemically comprehensive to account for the simultaneous and coupled homogeneous gas-phase and heterogeneous catalytic processes, it is imperative to develop reduced catalytic and gas-phase reaction mechanisms for hydrocarbon fuels for the large-scale simulations of turbulent, catalytic combustion systems.

In terms of prior contributions involving hetero-/homogeneous reactions and efforts towards their reduction, it is noted that the catalytic and gas-phase ignition temperatures of H₂/air mixtures over platinum were investigated numerically by Bui et al. [13] using reduced catalytic reaction mechanisms, which were developed based on the steady-state assumption for dominant

* Corresponding author.

E-mail address: rsui@princeton.edu (R. Sui).

surface species and reaction path analysis. It was reported that a reduced gas-phase reaction mechanism developed for gas-phase ignition had to be augmented by the H_2O_2 chemistry for the coupled hetero-/homogeneous combustion. In a subsequent study [14], Deshmukh and Vlachos reduced catalytic reaction mechanisms for fuel-lean CH_4 oxidation over platinum and rhodium, employing reaction path, sensitivity and partial equilibrium analyses. Reinke et al. [15,16] validated, by means of Raman and planar laser induced fluorescence measurements of OH, a set of detailed hetero-/homogeneous reaction mechanisms for the fuel-lean CH_4/air combustion over platinum and further provided a reduced catalytic mechanism [15] and a reduced gas-phase [16] mechanism valid at pressures 1 to 16 bar. It was also found that even in the absence of vigorous homogeneous combustion with flames, the gas-phase pre-ignition chemistry could contribute significantly to the CH_4 homogeneous conversion, especially at elevated pressures [16]. Yan and Maas [17] demonstrated a mathematical model allowing for the combined use of gas-phase and surface intrinsic low dimensional manifolds (ILDMs) in hetero-/homogeneous reacting flow calculations. Karadeniz et al. [18] reduced gas-phase methane and iso-octane mechanisms for application in catalytic partial oxidation. In view of these worthy contributions, it is nevertheless recognized that catalytic and gas-phase reaction mechanisms have not been systematically reduced *together* in hetero-/homogeneous combustion processes.

In the present study we shall therefore perform reduction of detailed catalytic and gas-phase reaction mechanisms *together* for the hetero-/homogeneous combustion of $\text{H}_2/\text{CO}/\text{O}_2/\text{N}_2$ mixtures over platinum. In choosing the $\text{H}_2/\text{CO}/\text{O}_2/\text{N}_2$ mixtures as a prototype to demonstrate the importance of the coupling in the reduction, we note that such mixtures are representative of syngas, whose catalytic combustion is attracting extensive industrial interest as it facilitates reduced emissions in gas turbines [19–22], is suited for microscale portable power generation systems [23] and allows for emission control and enhanced combustion stability in automotive internal combustion engines [24].

Combined mechanism reduction was accomplished using a method derived from the directed relation graph (DRG) [25–27] for a wide range of operating conditions. The DRG method was developed based on the notion that many species and elementary reactions are weakly coupled during combustion processes and do not significantly affect the reaction rates of the major species; this has proven to be a straightforward and efficient method in reducing large gas-phase reaction mechanisms [25]. However, DRG has not yet been applied to pure catalytic or combined catalytic/gas-phase combustion. Thus, one of our objectives is also to demonstrate the capability of the reducing method derived from DRG in creating reduced hetero-/homogeneous reaction mechanisms, which can capture major species concentration profiles, homogeneous ignition distances and flame temperatures.

This paper is organized as follows. The adopted simulation methodology, using a 2-D Navier Stokes code for a catalytic channel geometry, and the principle of the reducing method, are briefly discussed in Section 2. Next, the performance of reduced catalytic and gas-phase mechanisms for the heterogeneous-only and coupled hetero-/homogeneous combustion of fuel-lean $\text{H}_2/\text{CO}/\text{O}_2/\text{N}_2$ mixtures over Pt are presented in Sections 3.1 and 3.2, respectively. Mechanism reduction under fuel-rich conditions is then addressed in Section 3.3. Exothermicity and catalytic ignition of the reduced mechanisms are discussed in Section 3.4. Finally, the main results are summarized in Section 4.

2. Methodology

In previous studies [28–30] the hetero-/homogeneous combustion of $\text{H}_2/\text{CO}/\text{O}_2/\text{N}_2$ mixtures over Pt was investigated experimen-

tally in a high-pressure, optically accessible catalytic channel flow reactor and numerically using a 2-D steady Navier-Stokes code with detailed catalytic and gas-phase chemical reaction mechanisms; details of the numerical model have been reported in [31]. The governing equations were discretized using a finite volume approach and solution was obtained iteratively using an ADI algorithm with a SIMPLER method for the pressure-velocity field. The coupling between the homogeneous and the heterogeneous phases was treated via a modified Newton method for the surface species coverage and the interfacial (gas-solid) gaseous species mass fractions [29–32]. The rectangular channel reactor comprised two 9-mm-thick horizontal $\text{Si}[\text{SiC}]$ ceramic plates having a streamwise length (x) of 300 mm and a lateral width (z) of 104 mm, and two 3-mm-thick vertical quartz windows that maintained a vertical separation of 7 mm (y) between the two plates [29,30]. The inner $300 \times 104 \text{ mm}^2$ ceramic plate surfaces were coated with a Pt layer using plasma vapor deposition, while the catalyst temperatures were controlled by a combined heating/cooling arrangement comprising two adjustable-power resistive coils in the rear plate sections and two cooling air jets in the front plate sections [28,29]. The catalyst temperatures were measured along the x - y symmetry plane of the channel by 12 S-type thermocouples for each plate, which were positioned 0.9 mm beneath the catalytically coated surfaces. 1-D Raman measurements of the concentrations of the major gaseous species over the 7 mm channel height accessed the catalytic processes, while gas-phase combustion was monitored with planar laser induced fluorescence (PLIF) of OH for all fuel-lean stoichiometries and for the fuel-rich stoichiometries at pressures below ~5 bar. Hot-O₂ PLIF was used for fuel-rich cases at pressures above ~5 bar due to the associated ultra-low OH levels and the enhanced collisional quenching of the OH fluorescence signal [30,32].

Studies were performed at fuel-lean and fuel-rich global equivalence ratios of $\varphi = 0.13\text{--}7.0$ (based on both H_2 and CO fuel components), with and without the onset of gas-phase ignition, $\text{H}_2:\text{CO}$ molar ratios of 1:4.6–5:1 and pressures of 1–14 bar. The detailed catalytic reaction mechanism of H_2/CO oxidation on Pt from Zheng et al. [28] was employed in the simulations (25 irreversible and 2 reversible reactions, 9 surface and 8 gaseous species, which was based on an earlier $\text{CH}_4/\text{H}_2/\text{CO}$ mechanism by Deutschmann et al. [33]; see Table A1 in the Appendix). For the gas-phase chemistry, an elementary C1 scheme combining H_2/O_2 reactions from Burke et al. [34] and CO/O_2 reactions from Li et al. [35] was used (36 reversible reactions and 13 gaseous species, see Table A2 in the Appendix). Good agreements were established between the Raman/PLIF measurements and the predictions [28–30], thus attesting the adequacy of the employed detailed hetero-/homogeneous syngas chemical reaction mechanisms.

In the present work, simulations were performed using either detailed or reduced mechanisms. Selected cases from [28–30] that covered a wide range of operating conditions are summarized in Table 1. A staggered grid of 480×100 points, in x - and y -direction, respectively, for the $300 \times 7 \text{ mm}^2$ (x - y) channel domain along the symmetry plane $z = 0$ provided grid-independent solutions. It is noted that at far upstream locations ($x < 20 \text{ mm}$) the radical boundary layers are steep (however, with O and H mole fractions below $\sim 10^{-8}$) and need finer grid points to resolve. Temperature axial profiles at the lower ($y = 0$) and upper ($y = 7 \text{ mm}$) channel walls were constructed by fitting curves through the 12 thermocouple measurements and served as energy boundary conditions in the simulations. The gas mixture temperature, axial velocity and gaseous species mole fractions were uniform at the inlet, assessed by an inlet thermocouple and four mass flowmeters. Gas-phase and catalytic reaction rates were evaluated with Chemkin [36] and Surface-Chemkin [37], respectively. Mixture-averaged diffusion including thermal diffusion for the light species H_2

Table 1
Simulation conditions*.

Case	p	φ	T_{IN}	U_{IN}	H_2	CO	O_2	CO_2	$H_2:CO$
1	5	0.13	305	1.22	1.5	7.0	31.1	—	1:4.6
2	5	0.26	317	0.74	7.2	7.2	27.4	—	1:1
3	2	0.29	441	3.23	7.0	1.5	14.7	13.9	4.6:1
4	4	0.21	555	2.97	3.2	3.2	15.2	14.3	1:1
5	12	0.19	719	1.70	5.4	1.4	17.9	15.0	3.9:1
6	1	5.0	333	5.0	44.2	22.1	6.6	—	2:1
7	7	7.0	336	0.9	62.3	12.5	5.3	—	5:1
8	14	5.0	375	0.3	44.2	8.8	5.3	—	5:1

* Pressure (bar), global equivalence ratio, inlet temperature (K), inlet velocity (m/s), H_2 , CO, O_2 and CO_2 inlet vol.% content (the balance is N_2), and $H_2:CO$ volumetric ratio. Cases 1 and 2 from [29], 3–5 from [28] and 6–8 from [30].

and H were used in conjunction with the Chemkin Transport database [38].

The detailed catalytic and gas-phase reaction mechanisms were reduced based on the principle of directed relation graph (DRG) method [25–27]. Similar to the original DRG method, starting from a user-specified important Species A, the normalized contribution of the i -th reaction that involves Species B (but not the contribution of all B-related reactions) to the total production/destruction of A under a given condition can be defined as:

$$r_{AB}^i \equiv \frac{|\nu_{A,i}\omega_i\delta_{B,i}|}{\sum_{i=1,I} |\nu_{A,i}\omega_i|},$$

$$\delta_{B,i} = \begin{cases} 1, & \text{if the } i\text{-th reaction involves species B} \\ 0, & \text{otherwise} \end{cases} \quad (1)$$

where $\nu_{A,i}$ and ω_i , respectively, denote the stoichiometric coefficient of Species A and the reaction rate expressed in unit mol/cm³s for the i -th gaseous reaction. The catalytic reaction rate \dot{s}_i has the unit of mol/cm²s and is converted to the same dimension as ω_i by multiplying it by the reactor surface-to-volume ratio S/V . Unimportant reactions under a particular reaction condition are eliminated if $r_{AB}^i < \varepsilon$, where ε is a user-specified small-threshold relative error. All species that are not involved in any remaining reactions will be removed from the reduced mechanism.

The model reduction was performed using the surface perfectly stirred reactor (SPSR) [39] with detailed catalytic and gas-phase reaction mechanisms, mimicking the operating conditions in the real simulations. The SPSR simulations require only a few seconds to obtain convergent solutions. Due to the small-scale reactor geometry and the catalytic-dominant operating conditions in typical catalytic channels with known surface temperatures and inlet properties, a single sampling was shown quite satisfactory for the parametric space of the model reduction. The sampling included inlet gas composition, pressure, inlet temperature and residence time (channel length divided by inlet velocity) taken from Table 1, while the fitted thermocouple-measured wall temperature profiles were averaged for each case and then used as the SPSR surface temperature. Surface-to-volume ratio of the SPSR was kept the same as the channel catalytic reactor ($S/V = 2.85 \text{ cm}^{-1}$). The production/destruction rates of each reaction for every species were given by the SPSR calculation. Starting from the target Species A, all reactions (either catalytic or gas-phase) with a significant contribution ($r_{AB}^i > \varepsilon$) to A's production/destruction and the related Species B (and C, D, ... if any) were kept in the reduced mechanism. Same procedure was repeated for Species B and all the following related species until no more reactions (and species) could be added to the reduced scheme.

As the reductions were performed using an SPSR, transport effects were not considered. However, subsequent full 2-D simulations (with mixture-averaged diffusion including thermal diffusion for the light species) using the reduced mechanisms reproduced

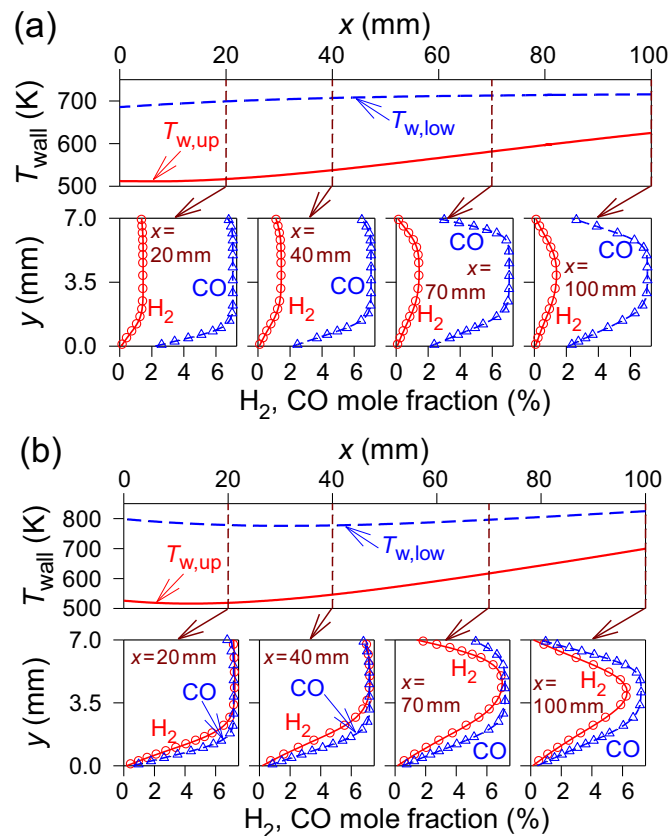


Fig. 1. Measured wall temperatures from [29] (solid lines: upper wall, dashed lines: lower wall) for Cases 1 (a) and 2 (b) in Table 1. For the same cases, predicted transverse profiles of H_2 (solid lines and circles) and CO (dashed lines and triangles) mole fractions are given at four selected axial locations. Lines denote results obtained using the detailed reaction mechanisms and symbols using the reduced reaction mechanisms.

very well the results of detailed mechanisms, indicating that transport did not significantly affect the chemistry reduction for the investigated channel geometry and operating conditions.

3. Results and discussion

3.1. Fuel-lean heterogeneous combustion

The catalytic and gas-phase reaction mechanisms were initially reduced together for Cases 1 and 2 in Table 1 using the reduction method described in Section 2. It is desired to reduce catalytic and gas-phase mechanisms jointly, as these two pathways are coupled via chemical, thermal and transport interactions. If catalytic and gas-phase reaction mechanisms are reduced separately, chemical coupling between the two reaction pathways will not be considered and automatically filtered out in the reduced mechanisms. H_2 was selected as the “starting species A” in the reduction procedure and the relative threshold error was $\varepsilon = 1\%$.

Due to the low inlet gas and surface temperatures, especially at the upper wall (see Fig. 1), vigorous gas-phase combustion was not initiated, as manifested by either the OH-PLIF measurements or the detailed-chemistry numerical simulations. The reduced model comprised of 13 catalytic reactions (S1, S4, S5, S8, S9, S14–S19, S22 and S24, see Table A1) and zero gas-phase reactions, leading to the elimination of ~80% of the detailed reactions and confirming the negligible importance of gas-phase chemistry for both Cases 1 and 2. Specifically, the gaseous species H, O, OH, HCO, CH_2O , N_2 and the surface species C(s) were removed (see Table A3).

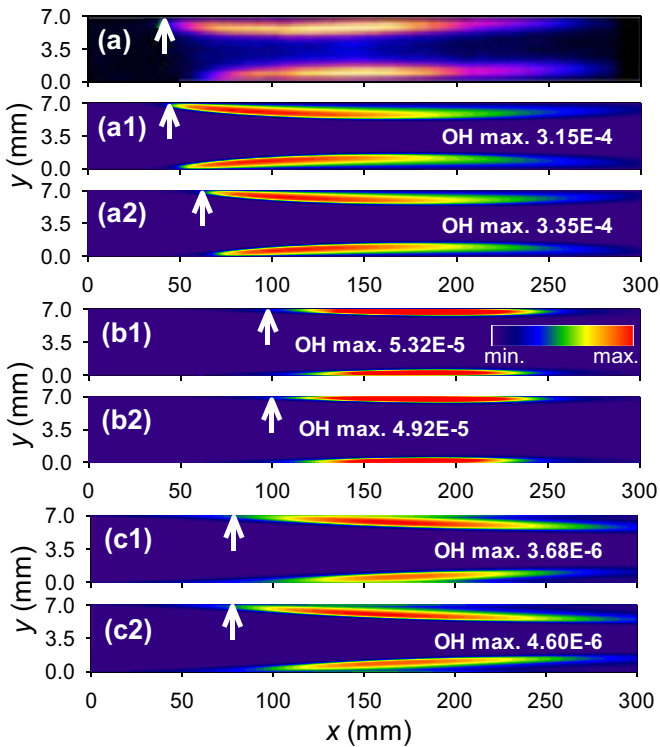


Fig. 2. PLIF-measured 2-D OH distribution for Case 3 ((a), adapted from [28]) and predicted 2-D OH mole fraction distributions for Cases 3-5: simulations obtained with the detailed reaction mechanisms (a1), (b1), and (c1) and the reduced reaction mechanisms (a2), (b2) and (c2). The vertical arrows denote the onset of homogeneous ignition.

Comparisons between predicted transverse profiles of H₂ and CO at selected axial locations $x = 20, 40, 70$ and 100 mm using detailed and reduced reaction mechanisms are provided in Fig. 1. In both cases, the reduced mechanism excellently reproduces the H₂ and CO mole fractions and the near-wall bending of the transverse profiles, which is directly linked to the local catalytic reactivity.

3.2. Fuel-lean hetero-/homogeneous combustion

Simulations were subsequently performed using either the detailed or the reduced mechanisms for Cases 3-5, in which gas-phase reactions were initiated. In these cases, CO₂ was added in the reactant stream (see Table 1) to control the homogeneous ignition location. Catalytic and gas-phase reaction mechanisms were reduced for Cases 3-5 following the same procedure as in Section 3.1.

The reduced mechanism for Case 3 included 22 catalytic and 12 gas-phase reactions (S1, S3-19, S22-S24, S26, R1, R4-R5, R11, R14-R18, R22, R23 and R27), while species HCO, CH₂O, and C(s) were neglected. The onset of homogeneous ignition (indicated by vertical arrows in Fig. 2) was defined as the far-upstream axial location where the OH mole fractions reached 5% of their maximum levels in the entire channel. It is seen that the gaseous combustion of H₂ is initiated first, while gaseous combustion of CO commences shortly downstream as the gas-phase oxidation of CO relies on the availability of the OH radical produced by the H₂ chemistry (R27: CO + OH = CO₂ + H). The 2-D OH distributions of Case 3 obtained via the PLIF measurement in [28] are shown in Fig. 2(a), while simulations using the detailed and reduced mechanisms are shown in Fig. 2(a1) and (a2), respectively.

The measured upper and lower wall temperatures for Case 3 are illustrated in Fig. 3(a). It is seen that two separate flame

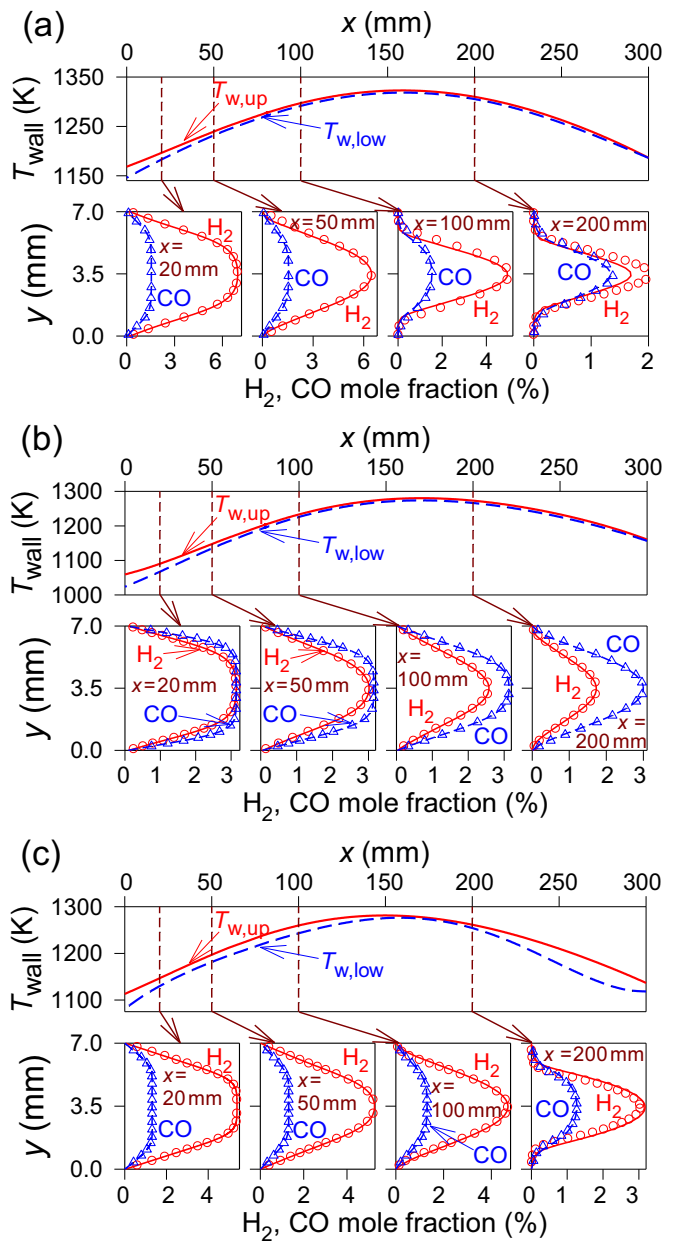


Fig. 3. Measured wall temperatures and predicted transverse profiles of H₂ and CO mole fractions at four selected axial locations for Cases 3-5, (a)-(c) in Table 1. Notations as in Fig. 1.

branches are established near the catalytic walls in Fig. 2(a), (a1), and (a2), due to the sub-unity Lewis number of the H₂ fuel component ($L_e H_2 \approx 0.3$): mass transport of H₂ towards the hot catalytic walls is faster than heat transfer away from walls, leading to the confinement of the resultant flames in the wall vicinity [40]. The reduced set of gaseous reactions modestly overestimates the homogeneous ignition distance, by 14 mm. Consequently, the reduced mechanism slightly underestimates the consumption of H₂ near both walls as evidenced by comparing results of the two simulations at $x = 50$ mm in Fig. 3(a). Since the reduced catalytic mechanism captures the transport-limited conversion of H₂ and CO at locations preceding the onset of homogeneous ignition (see Fig. 3(a) at $x = 20$ mm), the post homogeneous ignition differences in the H₂ profiles manifest a somewhat slower reduced gas-phase reaction model. This minor discrepancy is progressively aggravated at locations farther downstream in Fig. 3(a), especially at $x = 200$ mm.

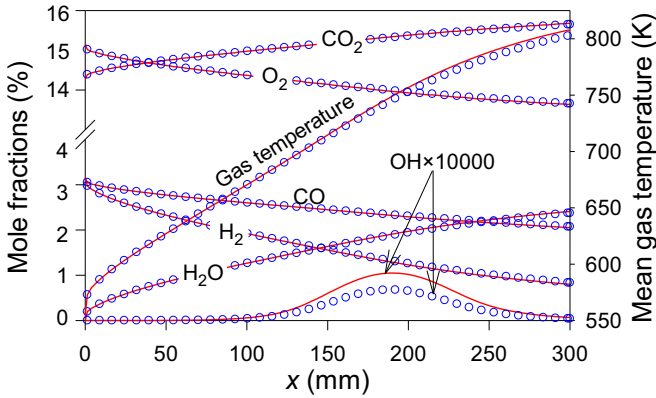


Fig. 4. Axial profiles of transversely-averaged mole fractions of major gaseous species, OH radical and gas temperature for Case 4. Lines denote results obtained using the detailed reaction mechanisms and symbols using the reduced reaction model.

It is seen that the OH mole fraction decreases significantly with increasing pressure at 4 bar in Case 4 and 12 bar in Case 5 (see OH peak values in Fig. 2(b1), and (b2) and (c1), and (c2)), due to their strong pressure dependence as discussed in [32]. The reduced mechanisms for the higher-pressure Cases 4 and 5 are smaller in size than the reduced mechanism for Case 3 and capture very well the OH distributions (see Fig. 2(b2), and (c2)) as well as the transverse profiles of H_2 and CO mole fractions (see Fig. 3(b), and (c)). The surface adsorption of the gas-phase radicals H (S3) and O (S7) is removed successively in the reduced mechanisms of Cases 4 and 5. The reduced mechanism for Case 4 comprises 21 catalytic and 10 gas-phase reactions (S1, S4–19, S22–S24, S26, R1, R4–R5, R11, R14–R18 and R27), while the one for Case 5 comprises 20 catalytic and 10 gas-phase reactions (S1, S4–S6, S8–19, S22–S24, S26, R1, R4–R5, R11, R15–R18, R23 and R27). In addition, very favorable comparisons of transversely-averaged mole fractions of major gaseous species, OH radical and gas temperature are obtained, as shown in Fig. 4 for Case 4.

3.3. Fuel-rich hetero-/homogeneous combustion

The applicability of the applied methodology of Section 2 in reducing the mechanisms for the hetero-/homogeneous combustion of fuel-rich $H_2/CO/O_2/N_2$ mixtures over Pt is examined with Cases 6–8. The OH mole fraction becomes ultra-low at fuel-rich conditions and decreases drastically with increasing pressure, thus rendering OH-PLIF not suitable for the detection of gaseous combustion at pressures above ca. 5 bar. For example, it was shown [32] that the equilibrium OH mole fraction at 1 bar of a fuel-rich ($\varphi = 5.06$) H_2 /air mixture was 3 orders of magnitude lower than that of a fuel-lean H_2 /air mixture having the same adiabatic temperature ($\varphi = 0.39$). This outcome in combination with the enhanced collisional quenching of the fluorescence signal at elevated pressures necessitated the use of hot- O_2 -PLIF in order to detect homogeneous ignition and flame formation [30,32] and hence to validate the detailed hetero-/homogeneous reaction mechanisms above 5 bar. Nonetheless, in the present numerical studies the homogeneous ignition was still defined by the OH radical for all pressures.

The model reduction for Case 6 at atmospheric pressure followed the similar procedure as the foregoing fuel-lean studies, while the deficient reactant O_2 was used as the “starting species A”. The user-specified small-threshold relative error ε was as low as 1×10^{-4} , otherwise catalytic and gas-phase reactions would become “decoupled” and all gas-phase reactions would be eliminated after the reduction. This strict threshold relative error of

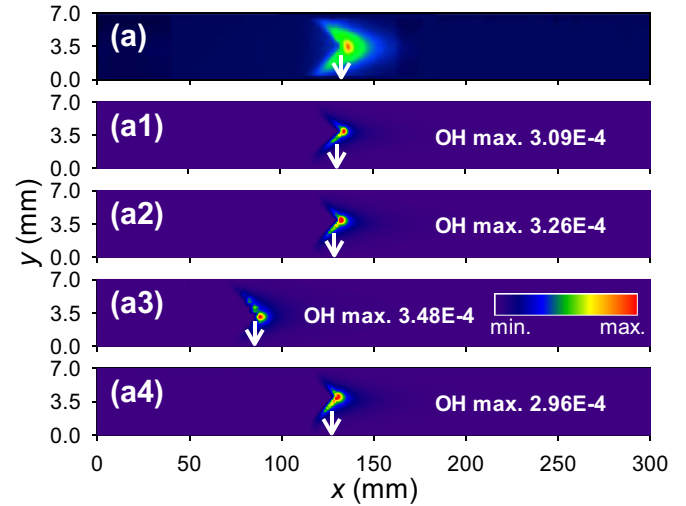


Fig. 5. PLIF-measured (a) (adapted from [30]) and predicted 2-D OH mole fraction distributions for Case 6 at 1 bar, obtained with the detailed reaction mechanisms (a1), reduced mechanism RM1 (a2), reduced mechanism RM2 (a3) and reduced mechanism RM2 supplemented by Reaction S3 (a4). The vertical arrows denote the onset of homogeneous ignition.

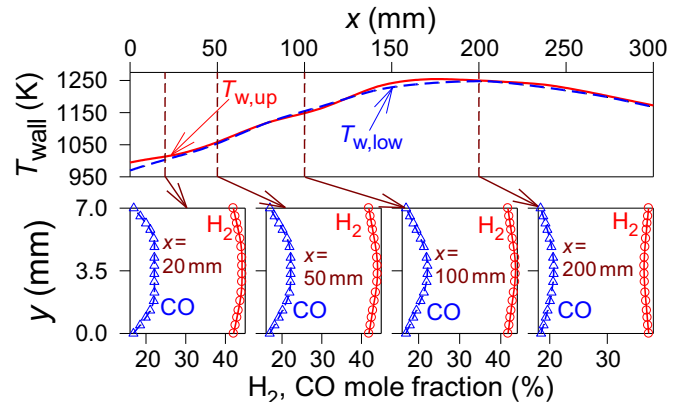


Fig. 6. Measured wall temperatures and predicted (using RM1) transverse profiles of H_2 and CO mole fractions at four selected axial locations for Case 6. Notations as in Fig. 1.

$\varepsilon = 1 \times 10^{-4}$ led to a rather large reduced mechanism (RM1) of 24 catalytic and 20 gas-phase reactions (S1–S5, S7–S24, S26, R1–R5, R11–R13, R15, R18, R20 and R22–R30). The reduced mechanism RM1 captured well the onset of homogeneous ignition (see Fig. 5(a)–(a2)) and the transverse profiles of H_2 and CO (see Fig. 6). The negative/positive gradients of the H_2 mole fraction profile at the lower/upper catalytic walls at the last selected axial location $x = 200$ mm (downstream of the flame) in Fig. 6 indicated H_2 catalytic production and was a result of catalytic splitting of the homogeneously-produced water (reaction sequence: S8, inverse S14 and S2) [30]. It is further noted that, contrary to the two separate flame branches of the fuel-lean studies in Fig. 2, the fuel-rich flames in Fig. 5 are V-shaped and closed, extending transversely (in y -direction) over the entire channel height, similar to fuel-lean hydrocarbon flames [16]. This is due to the larger-than unity Lewis number of the deficient reactant O_2 ($Le_{O_2} \approx 2$ at fuel-rich conditions).

In an attempt to achieve a more efficient reduction, detailed catalytic and gas-phase reaction mechanisms were also reduced not together but separately, both with a threshold of $\varepsilon = 1\%$ (as in Sections 3.1 and 3.2). The resulting reduced mechanism RM2

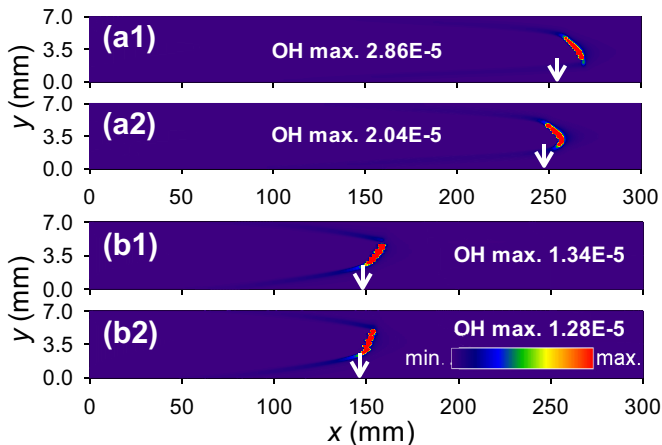


Fig. 7. Predicted 2-D OH mole fraction distributions for Cases 7–8: obtained with the detailed reaction mechanisms (a1)–(b1) and the reduced reaction mechanisms (a2)–(b2).

had 16 catalytic and 15 gas-phase reactions (S1–S2, S4–S5, S8–S9, S12, S14–S19, S22–S23, S26, R1–R4, R11–R13, R18, R20 and R25–R30). As shown in Fig. 5(a3), RM2 significantly underpredicted the homogeneous ignition distance. The reason is that during the coupled hetero-/homogeneous combustion, gas-phase ignition is controlled by two main coupling mechanisms with the catalytic reaction pathway, i.e. net radical (H, O and OH) transport to/from the surface and heat transfer from the hot surface to the colder gas. For Case 6, using RM2 only the non-kinetic thermal impact due to heat transfer from the hot surface to the gas is considered in the simulation, while the “bridge reactions” (Reactions S3, S7, S10–11, especially the surface adsorption of H radicals via S3) are ignored, thus leading to the incorrect prediction of homogeneous ignition. As shown in Fig. 5(a4), the simulation using RM2 supplemented by S3 recovered the correct homogeneous ignition distance.

At higher pressures, however, the impact of the radical transport to/from the catalytic surfaces on the gas-phase combustion was progressively reduced. Characteristically, for Cases 7 and 8 at 7 bar and 14 bar, respectively, the threshold value ε had to be reduced to 1×10^{-8} to maintain the “bridge reactions” and the ensuing gas-phase reactions during the model reduction, resulting in mechanisms that basically could not be reduced. This indicates negligible importance of the gas-surface radical transport in the homogeneous ignitions. Thus, detailed catalytic and gas-phase reactions were again reduced separately for Cases 7 and 8, following the same procedure as the previously mentioned RM2 for Case 6, using the threshold $\varepsilon = 1\%$. The reduced mechanism for Case 7 had 16 catalytic and 17 gas-phase reactions (S1–S2, S4–S5, S8–S9, S12, S14–S19, S22–S23, S26, R1–R4, R11–R13, R16, R18–R20, R26–R30 and R34), while that for Case 8 had 16 catalytic and 18 gas-phase reactions (S1–S2, S4–S5, S8–S9, S12, S14–S19, S22–S23, S26, R1–R4, R11–R13, R16–R20, R26–R30 and R34). Both reduced mechanisms captured well the ignition of gaseous combustion (see Fig. 7) and excellently reproduced the transverse profiles of H₂ and CO mole fractions at various axial locations (see Fig. 8).

The strict threshold 1×10^{-4} of Case 6 in order to include gas-phase reactions was due to the weak impact of OH radical (via S11) on the summed absolute construction/destruction $\sum_{i=1,I} |v_{A,i}\omega_i|$ of OH(s), which was in turn linked to the starting species O₂ via O(s) in the directed relation graph. Looking from the opposite direction, OH(s) via S11 contributed 44% of OH's summed absolute construction/destruction. If OH was chosen as the starting species A for the reduction procedure, appreciably less strict threshold value would be required for the reduction. However, we do not sug-

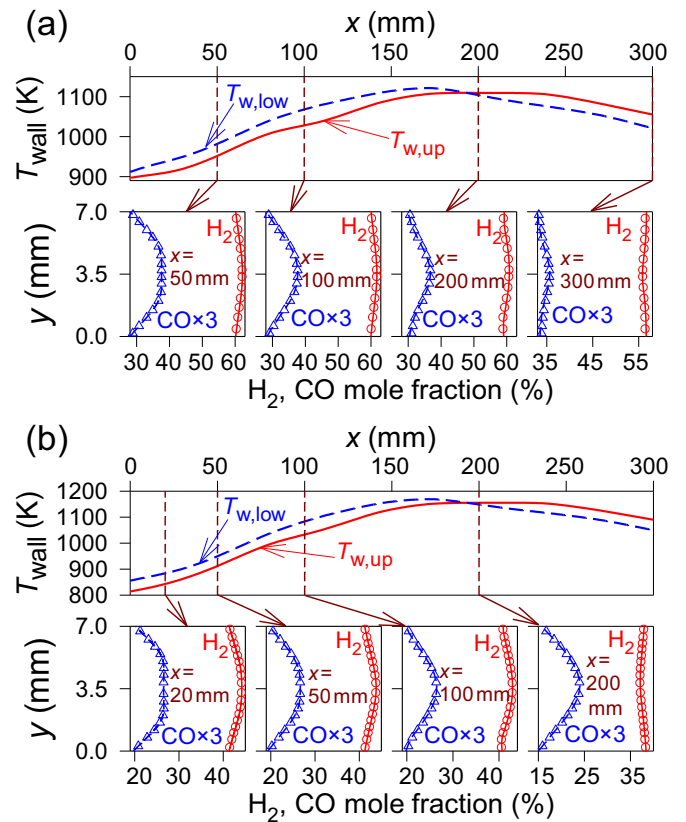


Fig. 8. Wall temperatures and predicted transverse profiles of H₂ and CO mole fractions at four selected axial locations for Cases 7–8. Notations as in Fig. 1.

gest choosing radicals or any minor species as the starting species for mechanism reduction in real applications, because it is often unknown prior to full simulations or experiments whether gas-phase combustion is ignited, and when gas-phase combustion is ignited, whether surface-gas radical transport is important. In the cases where gas-phase combustion is not ignited (e.g. Cases 1–2) or surface-gas radical transport does not play an important role in the ignition of gas-phase chemistry (e.g. Cases 7–8), using radicals or other minor species as the (automatically reserved) starting species will result in inefficient mechanism reduction.

For large-scale simulations of turbulent catalytic combustion, the strategy is to perform the reduction in a suitable laminar configuration (such as the present catalytic channel geometry) using detailed hetero-/homogeneous mechanisms and selected operating conditions of pressure, temperature, and equivalence ratio. The reduced mechanisms could be subsequently applied to computationally expensive turbulent simulations under similar operating conditions.

3.4. Surface exothermicity and catalytic ignition of the reduced mechanisms

In the catalytic channel flow reactor simulated in Sections 3.1–3.3, the surface temperatures were prescribed and hence the surface exothermicity was not studied. The validity of the reduced hetero-/homogeneous mechanisms in the case of non-prescribed surface temperature is addressed in this Section. Specifically, using DRG-based methods, a parametric space is first sampled, including the reactant composition, pressure, residence time, inlet temperature and reactor temperature. The important species and reactions are determined accordingly based on their

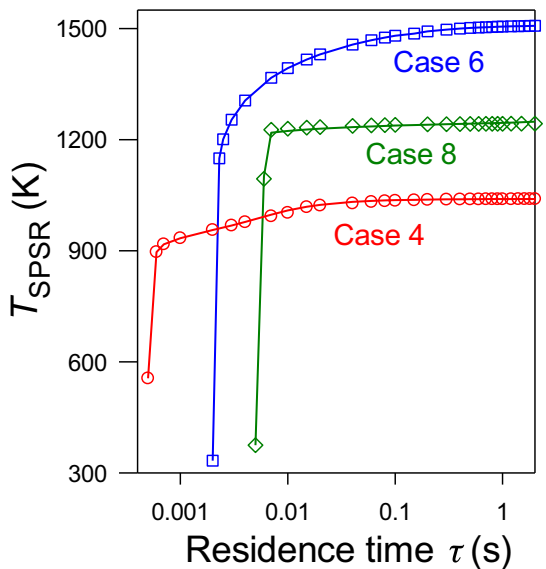


Fig. 9. Predicted SPSR temperature T_{SPSR} versus residence time τ for Cases 4, 6 and 8 using the detailed (lines) and reduced (symbols) reaction mechanisms. Simulation conditions (except for residence time) were taken from Table 1.

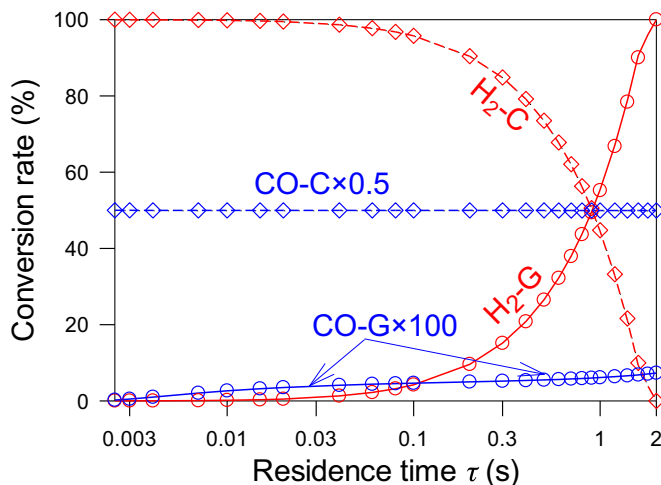


Fig. 10. SPSR predicted gaseous (G, solid lines and circles) and catalytic (C, dashed lines and diamonds) conversion rates of H_2 and CO for Case 6 at various residence time τ using the detailed (lines) and reduced (symbols) reaction mechanisms.

direct and indirect contributions to the consumption/destruction of the important species, e.g. hydrogen in fuel-lean cases and oxygen in fuel-rich cases as in Sections 3.1–3.3. Nonetheless, the reduced mechanisms can also be used for predicting systems with surface exothermicity.

Simulations were performed using the SPSR [39] under *adiabatic* condition for three selected cases mimicking Cases 4, 6 and 8. For each case, inlet reactant composition, pressure and inlet temperature were kept the same as in Table 1, while the residence time was varied from 0.0005 s to 2 s. Fig. 9 shows the simulated ignition process at various residence times. As shown in Fig. 9 for all selected cases, the reduced mechanisms developed in Sections 3.2 and 3.3 captured very well the catalytic ignition and heat release for all residence times. In addition, the computed catalytic and gaseous conversions of H_2 and CO for Case 6 using both detailed and reduced mechanisms are compared in Fig. 10. The favorable comparison of both catalytic and gaseous fuel conversions,

together with the well reproduced reactor temperatures that is due to the exothermicity of both reaction pathways, indicate that both catalytic and gaseous exothermicities are properly captured using the reduced mechanism.

4. Conclusions

Detailed catalytic and gas-phase reaction mechanisms for the hetero-/homogeneous combustion of $\text{H}_2/\text{CO}/\text{O}_2/\text{N}_2$ mixtures over Pt were reduced using a method derived from the directed relation graph (DRG) for a wide range of operating conditions. Simulations were performed in a Pt-coated planar channel using a 2-D steady Navier Stokes code with both detailed and reduced mechanisms for various global equivalence ratios, $\text{H}_2:\text{CO}$ volumetric ratios, pressures, surface temperatures and inlet gas temperatures. The following are the key conclusions obtained herein.

- (1) At fuel-lean conditions for both heterogeneous-only and hetero-/homogeneous combustion, catalytic and gas-phase reaction mechanisms can be treated as a single item and reduced together. This allows for the proper representation of the key hetero-/homogeneous chemical interactions.
- (2) At low-pressure fuel-rich conditions, very low threshold relative error is needed to accurately capture the homogeneous ignition, resulting in a relatively inefficient reduction. At high-pressure fuel-rich conditions, for a more efficient reduction the catalytic and gas-phase reaction mechanisms could be reduced separately, which does not sacrifice the accuracy of the reduced mechanisms due to the reduced importance of the gas-surface radical coupling.
- (3) The reduced mechanisms reproduce well the major gaseous species concentrations, gas temperatures and homogeneous ignition distances obtained with the detailed reaction mechanisms, thus demonstrating the applicability of the applied method in reducing mechanisms for hetero-/homogeneous combustion systems. It is also shown that for fuel-lean conditions, prior to full simulations, the reduction could provide a straightforward and rapid indication if gas-phase combustion is ignited, and the important reactions and contributions of both reaction pathways, and could further benefit the demanding large-scale numerical simulation for the design and thermal management of catalytic combustion systems.
- (4) Additional simulations in a surface perfectly stirred reactor (SPSR) shows that the reduced mechanisms could also predict surface exothermicity and catalytic ignition for problems without prescribed surface temperature.

Declaration of Competing Interest

The authors declare that they have no known competing financial interests or personal relationships that could have appeared to influence the work reported in this paper.

Acknowledgments

RS acknowledges the financial support from the Swiss National Science Foundation EPM fellowship (Award Number 178619).

Appendix

Tables A1–A3.

Table A1

Detailed catalytic reaction mechanism of syngas oxidation over Pt and the reduced catalytic mechanisms*.

No.	Reaction	A	b	E _a	Reduced mechanisms							
					1	2	3	4	5	RM1	6	RM3
S1	H ₂ + 2Pt(s) → 2H(s)	4.46 × 10 ¹⁰	0.5	0	✓	✓	✓	✓	✓	✓	✓	✓
S2	2H(s) → 2Pt(s) + H ₂	3.70 × 10 ²¹	0	67.4–6 θ _{H(s)}						✓	✓	✓
S3	H + Pt(s) → H(s)	1.0 (γ)	0	0			✓			✓		✓
S4	O ₂ + 2Pt(s) → 2O(s)	1.80 × 10 ²¹	-0.5	0		✓	✓	✓	✓	✓	✓	✓
S5	O ₂ + 2Pt(s) → 2O(s)	0.023 (γ)	0	0		✓	✓	✓	✓	✓	✓	✓
S6	2O(s) → 2Pt(s) + O ₂	3.70 × 10 ²¹	0	213.2–60 θ _{O(s)}		✓	✓	✓		✓	✓	✓
S7	O + Pt(s) → O(s)	1.0 (γ)	0	0			✓	✓		✓		✓
S8	H ₂ O + Pt(s) → H ₂ O(s)	0.75 (γ)	0	0		✓	✓	✓	✓	✓	✓	✓
S9	H ₂ O(s) → Pt(s) + H ₂ O	1.00 × 10 ¹³	0	40.3		✓	✓	✓	✓	✓	✓	✓
S10	OH + Pt(s) → OH(s)	1.0 (γ)	0	0			✓	✓	✓	✓		✓
S11	OH(s) → Pt(s) + OH	1.00 × 10 ¹³	0	192.8			✓	✓	✓	✓		✓
S12	H(s) + O(s) → OH(s) + Pt(s)	3.70 × 10 ²⁰	0	70.5			✓	✓	✓	✓	✓	✓
S13	OH(s) + Pt(s) → H(s) + O(s)	1.00 × 10 ²¹	0	130.69			✓	✓	✓	✓		✓
S14	H(s) + OH(s) = H ₂ O(s) + Pt(s)	3.70 × 10 ²¹	0	17.4		✓	✓	✓	✓	✓	✓	✓
S15	2OH(s) = O(s) + H ₂ O(s)	3.70 × 10 ²¹	0	48.2		✓	✓	✓	✓	✓	✓	✓
S16	CO + Pt(s) → CO(s)	0.84 (γ)	0	0		✓	✓	✓	✓	✓	✓	✓
S17	CO(s) → Pt(s) + CO	2.13 × 10 ¹³	0	136.19–33θ _{CO(s)}		✓	✓	✓	✓	✓	✓	✓
S18	CO ₂ (s) → Pt(s) + CO ₂	1.00 × 10 ¹³	0	20.5		✓	✓	✓	✓	✓	✓	✓
S19	CO(s) + O(s) → CO ₂ (s) + Pt(s)	3.70 × 10 ²⁰	0	108.0–33θ _{CO(s)}		✓	✓	✓	✓	✓	✓	✓
S20	C(s) + O(s) → CO(s) + Pt(s)	3.70 × 10 ²¹	0	62.80						✓		
S21	CO(s) + Pt(s) → C(s) + O(s)	1.00 × 10 ¹⁸	0	184.0						✓		
S22	CO(s) + OH(s) → HCOO(s) + Pt(s)	3.70 × 10 ²¹	0	94.2		✓	✓	✓	✓	✓	✓	✓
S23	HCOO(s) + Pt(s) → CO(s) + OH(s)	1.33 × 10 ²¹	0	0.87			✓	✓	✓	✓	✓	✓
S24	HCOO(s) + O(s) → CO ₂ (s) + OH(s)	3.70 × 10 ²¹	0	0		✓	✓	✓	✓	✓	✓	✓
S25	CO ₂ (s) + OH(s) → HCOO(s) + O(s)	2.79 × 10 ²¹	0	151.05						✓		
S26	HCOO(s) + Pt(s) → CO ₂ (s) + H(s)	3.70 × 10 ²¹	0	0			✓	✓	✓	✓	✓	✓
S27	CO ₂ (s) + H(s) → HCOO(s) + Pt(s)	2.79 × 10 ²¹	0	90.05						✓		

* Reaction rates are $k = A\Gamma^b \exp(E_a/RT)$ with A (mol·cm·K·s) and E_a (kJ/mol). The surface site density is $\Gamma = 2.7 \times 10^{-9}$ mol/cm² and γ denotes sticking coefficients. Reactions S4 and S5 are duplicate. S1 and S2 have orders of one and two with respect to Pt(s), respectively. "✓" marks remaining reactions in the reduced reaction mechanisms.

Table A2

Detailed gas-phase reaction mechanism of syngas oxidation and the reduced gas-phase mechanisms*.

No.	Reaction	A	B	E _a	Reduced mechanisms							
					1	2	3	4	5	RM1	6	RM3
R1	H + O ₂ = O + OH	1.04 × 10 ¹⁴	0	63.96	✓	✓	✓	✓	✓	✓	✓	✓
R2	O + H ₂ = H + OH	3.82 × 10 ¹²	0	33.25						✓	✓	✓
R3	O + H ₂ = H + OH	8.79 × 10 ¹⁴	0	80.21						✓	✓	✓
R4	H ₂ + OH = H ₂ O + H	2.16 × 10 ⁸	1.51	14.35		✓	✓	✓	✓	✓	✓	✓
R5	2OH = O + H ₂ O	3.34 × 10 ⁴	2.42	-8.08						✓	✓	✓
R6	H ₂ + M = 2H + M	4.85 × 10 ¹⁹	-1.4	436.73		✓	✓	✓	✓	✓	✓	✓
R7	2O + M = O ₂ + M	6.15 × 10 ¹⁵	-0.5	0								
R8	O + H + M = OH + M	4.71 × 10 ¹⁸	-1.0	0								
R9	H ₂ O + M = H + OH + M	6.06 × 10 ²⁷	-3.32	505.39								
R10	2H ₂ O = H + OH + H ₂ O	1.01 × 10 ²⁶	-2.44	502.83								
R11	H + O ₂ (+M) = HO ₂ (+M)	4.65 × 10 ¹²	0.44	0		✓	✓	✓	✓	✓	✓	✓
		6.37 × 10 ²⁰	-1.72	2.20								
R12	HO ₂ + H = H ₂ + O ₂	2.75 × 10 ⁶	2.09	-6.07						✓	✓	✓
R13	HO ₂ + H = 2OH	7.08 × 10 ¹³	0	1.23						✓	✓	✓
R14	HO ₂ + O = O ₂ + OH	2.85 × 10 ¹⁰	1.0	-3.03		✓	✓					
R15	HO ₂ + OH = H ₂ O ₂ + O ₂	2.89 × 10 ¹³	0	-2.08		✓	✓	✓	✓			
R16	2HO ₂ = H ₂ O ₂ + O ₂	4.20 × 10 ¹⁴	0	50.13		✓	✓	✓	✓			
R17	2HO ₂ = H ₂ O ₂ + O ₂	1.30 × 10 ¹¹	0	-6.82		✓	✓	✓	✓			
R18	HO ₂ (+M) = 2OH (+M)	2.00 × 10 ¹²	0.9	203.97		✓	✓	✓	✓	✓	✓	✓
		2.49 × 10 ²⁴	-2.3	203.97								
R19	H ₂ O ₂ + H = H ₂ O + OH	2.41 × 10 ¹³	0	16.61								
R20	H ₂ O ₂ + H = HO ₂ + H ₂	4.82 × 10 ¹³	0	33.26						✓	✓	✓
R21	H ₂ O ₂ + O = OH + HO ₂	9.55 × 10 ⁶	2.0	16.61								
R22	H ₂ O ₂ + OH = HO ₂ + H ₂ O	1.74 × 10 ¹²	0	1.33		✓				✓		
R23	H ₂ O ₂ + OH = HO ₂ + H ₂ O	7.59 × 10 ¹³	0	30.42		✓		✓				
R24	CO + O (+M) = CO ₂ (+M)	1.80 × 10 ¹⁰	0	9.96						✓		
		1.55 × 10 ²⁴	-2.7	17.53								
R25	CO + O ₂ = CO ₂ + O	2.53 × 10 ¹²	0	199.58						✓	✓	✓
R26	CO + HO ₂ = CO ₂ + OH	3.01 × 10 ¹³	0	96.23						✓	✓	✓

(continued on next page)

Table A2 (continued)

No.	Reaction	A	B	E_a	Reduced mechanisms								
					1	2	3	4	5	6	RM1	RM2	RM3
R27	$\text{CO} + \text{OH} = \text{CO}_2 + \text{H}$	2.23×10^5	1.9	-4.85							✓	✓	✓
R28	$\text{HCO} + \text{M} = \text{H} + \text{CO} + \text{M}$	4.75×10^{11}	0.7	62.34							✓	✓	✓
R29	$\text{HCO} + \text{O}_2 = \text{CO} + \text{HO}_2$	7.58×10^{12}	0	1.72							✓	✓	✓
R30	$\text{HCO} + \text{H} = \text{CO} + \text{H}_2$	7.23×10^{13}	0	0							✓	✓	✓
R31	$\text{HCO} + \text{O} = \text{CO} + \text{OH}$	3.02×10^{13}	0	0									
R32	$\text{HCO} + \text{O} = \text{CO}_2 + \text{H}$	3.00×10^{13}	0	0									
R33	$\text{HCO} + \text{OH} = \text{CO} + \text{H}_2\text{O}$	3.02×10^{13}	0	0									
R34	$\text{HCO} + \text{HO}_2 = \text{CO}_2 + \text{OH} + \text{H}$	3.00×10^{13}	0	0									✓
R35	$2\text{HCO} = \text{H}_2 + 2\text{CO}$	3.00×10^{12}	0	0									
R36	$2\text{HCO} = \text{CH}_2\text{O} + \text{CO}$	3.13×10^{13}	0	0									

* Reaction rates are $k = AT^b \exp(E_a/RT)$ with A (mol·cm-K-s) and E_a (kJ/mol). R2/R3, R16/R17 and R22/R23 are duplicate reactions. R11 and R18 are Troe reactions centered at 0.5 and 0.42, respectively, and R24 a pressure-dependent reaction (second entries are the low-pressure limits). Third body efficiencies in reactions R6–R8 are $\omega_{\text{H}_2\text{O}} = 12.0$, $\omega_{\text{H}_2} = 2.5$, $\omega_{\text{CO}} = 1.9$ and $\omega_{\text{CO}_2} = 3.8$; in R9: $\omega_{\text{H}_2\text{O}} = 0.0$, $\omega_{\text{H}_2} = 3.0$, $\omega_{\text{O}_2} = 1.5$, $\omega_{\text{CO}} = 1.9$, $\omega_{\text{CO}_2} = 3.8$ and $\omega_{\text{N}_2} = 2.0$; in R11: $\omega_{\text{H}_2\text{O}} = 14.0$, $\omega_{\text{H}_2} = 2.0$, $\omega_{\text{O}_2} = 0.78$, $\omega_{\text{CO}} = 1.9$, and $\omega_{\text{CO}_2} = 3.8$; in R18: $\omega_{\text{H}_2\text{O}} = 7.5$, $\omega_{\text{H}_2} = 7.7$, $\omega_{\text{O}_2} = 3.7$, $\omega_{\text{CO}} = 1.2$, $\omega_{\text{CO}_2} = 2.8$, $\omega_{\text{N}_2} = 1.5$; in R24: $\omega_{\text{H}_2\text{O}} = 12.0$, $\omega_{\text{H}_2} = 2.5$, $\omega_{\text{CO}} = 1.9$ and $\omega_{\text{CO}_2} = 3.8$; in R28: $\omega_{\text{H}_2\text{O}} = 6.0$, $\omega_{\text{H}_2} = 2.5$, $\omega_{\text{CO}} = 1.9$ and $\omega_{\text{CO}_2} = 3.8$. "✓" marks remaining reactions in the reduced reaction mechanisms.

Table A3
Surface and gaseous species in the reduced reaction mechanisms.

Species	Reduced mechanisms										
	1	2	3	4	5	6	RM1	RM2	RM3	7	8
H(s)	✓	✓	✓	✓	✓	✓	✓	✓	✓	✓	✓
O(s)	✓	✓	✓	✓	✓	✓	✓	✓	✓	✓	✓
OH(s)	✓	✓	✓	✓	✓	✓	✓	✓	✓	✓	✓
H ₂ O(s)	✓	✓	✓	✓	✓	✓	✓	✓	✓	✓	✓
CO(s)	✓	✓	✓	✓	✓	✓	✓	✓	✓	✓	✓
CO ₂ (s)	✓	✓	✓	✓	✓	✓	✓	✓	✓	✓	✓
C(s)						✓					
HCOO(s)	✓	✓	✓	✓	✓	✓	✓	✓	✓	✓	✓
Pt(s)	✓	✓	✓	✓	✓	✓	✓	✓	✓	✓	✓
H ₂	✓	✓	✓	✓	✓	✓	✓	✓	✓	✓	✓
CO	✓	✓	✓	✓	✓	✓	✓	✓	✓	✓	✓
O ₂	✓	✓	✓	✓	✓	✓	✓	✓	✓	✓	✓
H						✓	✓	✓	✓	✓	✓
O						✓	✓	✓	✓	✓	✓
OH						✓	✓	✓	✓	✓	✓
H ₂ O	✓	✓	✓	✓	✓	✓	✓	✓	✓	✓	✓
HO ₂	✓	✓	✓	✓	✓	✓	✓	✓	✓	✓	✓
H ₂ O ₂	✓	✓	✓	✓	✓	✓	✓	✓	✓	✓	✓
CO ₂	✓	✓	✓	✓	✓	✓	✓	✓	✓	✓	✓
HCO						✓	✓	✓	✓	✓	✓
CH ₂ O							✓	✓	✓	✓	✓
N ₂	✓	✓	✓	✓	✓	✓	✓	✓	✓	✓	✓

References

- [1] R.A. Dalla Betta, J.C. Schlatter, S.G. Nickolas, M.B. Cutrone, K.W. Beebe, Y. Furuse, T. Tsuchiya, Development of a catalytic combustor for a heavy-duty utility gas turbine, *J. Eng. Gas Turb. Power* 119 (1997) 844–851.
- [2] S. Eriksson, A. Schneider, J. Mantzaras, M. Wolf, S. Jaras, Experimental and numerical investigation of supported rhodium catalysts for partial oxidation of methane in exhaust gas diluted reaction mixtures, *Chem. Eng. Sci.* 62 (2007) 3991–4011.
- [3] M. Kumar, M. Bhandwal, M. Sharma, A. Verma, U. Srivastava, R.K. Tyagi, Effect of creating turbulence on the performance of catalytic converter, *Int. J. Perform. Eng.* 12 (2016) 115–120.
- [4] P. Biloen, W.M.H. Sachtler, Mechanism of hydrocarbon synthesis over Fischer-Tropsch catalysts, *Adv. Catal.* 30 (1981) 165–216.
- [5] K.W. Beebe, K.D. Cairns, V.K. Pareek, S.G. Nickolas, J.C. Schlatter, T. Tsuchiya, Development of catalytic combustion technology for single-digit emissions from industrial gas turbines, *Catal. Today* 59 (2000) 95–115.
- [6] M. Iwaniszy, J. Ochońska, P. Jodłowski, J. Łojewska, A. Matuszek-Chmurowska, A. Kołodziej, Microstructured reactor as a pre-turbo catalytic converter, *Top. Catal.* 56 (2013) 384–389.
- [7] H. Santos, M. Costa, Modelling transport phenomena and chemical reactions in automotive three-way catalytic converters, *Chem. Eng. J.* 148 (2009) 173–183.
- [8] H. Ström, S. Sasic, B. Andersson, Effects of the turbulent-to-laminar transition in monolithic reactors for automotive pollution control, *Ind. Eng. Chem. Res.* 50 (2011) 3194–3205.
- [9] H. Ström, S. Sasic, Heat and mass transfer in automotive catalysts—the influence of turbulent velocity fluctuations, *Chem. Eng. Sci.* 83 (2012) 128–137.
- [10] F. Lucci, C.E. Frouzakis, J. Mantzaras, Three-dimensional direct numerical simulation of turbulent channel flow catalytic combustion of hydrogen over platinum, *Proc. Combust. Inst.* 34 (2013) 2295–2302.
- [11] B.O. Arani, C.E. Frouzakis, J. Mantzaras, F. Lucci, K. Boulochos, Direct numerical simulation of turbulent channel-flow catalytic combustion: effects of Reynolds number and catalytic reactivity, *Combust. Flame* 187 (2018) 52–66.
- [12] B.O. Arani, C.E. Frouzakis, J. Mantzaras, K. Boulochos, Direct numerical simulations of turbulent catalytic and gas-phase combustion of H₂/air over Pt at practically-relevant Reynolds numbers, *Proc. Combust. Inst.* 37 (2019) 5489–5497.
- [13] P.A. Bui, E.A. Wilder, D.G. Vlachos, P.R. Westmoreland, Hierarchical reduced models for catalytic combustion: H₂/air mixtures near platinum surfaces, *Combust. Sci. Technol.* 129 (1997) 243–275.
- [14] S.R. Deshmukh, D.G. Vlachos, A reduced mechanism for methane and one-step rate expressions for fuel-lean catalytic combustion of small alkanes on noble metals, *Combust. Flame* 149 (2007) 366–383.
- [15] M. Reinke, J. Mantzaras, R. Schaeeren, R. Bombach, A. Inauen, S. Schenker, High-pressure catalytic combustion of methane over platinum: in situ experiments and detailed numerical predictions, *Combust. Flame* 136 (2004) 217–240.
- [16] M. Reinke, J. Mantzaras, R. Bombach, S. Schenker, A. Inauen, Gas phase chemistry in catalytic combustion of methane/air mixtures over platinum at pressures of 1bar to 16bar, *Combust. Flame* 141 (2005) 448–468.
- [17] X. Yan, U. Maas, Intrinsic low-dimensional manifolds of heterogeneous combustion processes, *Proc. Combust. Inst.* 28 (2000) 1615–1621.
- [18] H. Karadeniz, H.S. Soyhan, C. Sorusbay, Reduction of large kinetic mechanisms with a new approach to the necessity analysis method, *Combust. Flame* 159 (2012) 1467–1480.
- [19] J. Mantzaras, Catalytic combustion of syngas, *Combust. Sci. Technol.* 180 (2008) 1137–1168.
- [20] S. Blakey, L. Rye, C.W. Wilson, Aviation gas turbine alternative fuels: a review, *Proc. Combust. Inst.* 33 (2011) 2863–2885.
- [21] R. Sui, W. Liang, L. Zhang, J. Mantzaras, C.K. Law, Kinetic interactions between H₂ and CO in catalytic oxidation over PdO, *Combust. Flame* 211 (2020) 270–280.
- [22] E.S. Rubin, H. Mantripragada, A. Marks, P. Versteeg, J. Kitchin, The outlook for improved carbon capture technology, *Prog. Energy Combust. Sci.* 38 (2012) 630–671.
- [23] R. Sui, E. Es-sebbar, J. Mantzaras, N.I. Prasianakis, Experimental and numerical investigation of fuel-lean H₂/CO/air and H₂/CH₄/air catalytic microreactors, *Combust. Sci. Technol.* 190 (2018) 336–362.
- [24] A.J. Boehman, O. Corre, Combustion of syngas in internal combustion engines, *Combust. Sci. Technol.* 180 (2008) 1193–1206.
- [25] T. Lu, C.K. Law, A directed relation graph method for mechanism reduction, *Proc. Combust. Inst.* 30 (2005) 1333–1341.
- [26] T. Lu, C.K. Law, Linear time reduction of large kinetic mechanisms with directed relation graph: n-heptane and iso-octane, *Combust. Flame* 144 (2006) 24–36.
- [27] T. Lu, C.K. Law, On the applicability of directed relation graphs to the reduction of reaction mechanisms, *Combust. Flame* 146 (2006) 472–483.
- [28] X. Zheng, J. Mantzaras, R. Bombach, Homogeneous combustion of fuel-lean syngas mixtures over platinum at elevated pressures and preheats, *Combust. Flame* 160 (2013) 155–169.
- [29] X. Zheng, J. Mantzaras, R. Bombach, Kinetic interactions between hydrogen and carbon monoxide oxidation over platinum, *Combust. Flame* 161 (2014) 332–346.
- [30] M. Schultze, J. Mantzaras, F. Grygier, R. Bombach, Hetero-/homogeneous combustion of syngas mixtures over platinum at fuel-rich stoichiometries and pressures up to 14bar, *Proc. Combust. Inst.* 35 (2015) 2223–2231.
- [31] Y. Ghermay, J. Mantzaras, R. Bombach, K. Boulochos, Homogeneous combus-

- tion of fuel lean H₂/O₂/N₂ mixtures over platinum at elevated pressures and preheats, Combust. Flame 158 (2011) 1491–1506.
- [32] R. Sui, E. Es-sebbar, J. Mantzaras, R. Bombach, Homogeneous ignition during fuel-rich H₂/O₂/N₂ combustion in platinum-coated channels at elevated pressures, Combust. Flame 180 (2017) 184–195.
- [33] O. Deutschmann, L.I. Maier, U. Riedel, A.H. Stroemman, R.W. Dibble, Hydrogen assisted catalytic combustion of methane on platinum, Catal. Today 59 (2000) 141–150.
- [34] M.P. Burke, M. Chaos, Y. Ju, F.L. Dryer, S.J. Klippenstein, Comprehensive H₂/O₂ kinetic model for high-pressure combustion, Int. J. Chem. Kinet. 44 (2012) 444–474.
- [35] J. Li, Z.W. Zhao, A. Kazakov, M. Chaos, F.L. Dryer, J.J. Scire, A comprehensive kinetic mechanism for CO, CH₂O, and CH₃OH combustion, Int. J. Chem. Kinet. 39 (2007) 109–136.
- [36] R.J. Kee, F.M. Rupley, J.A. Miller, Chemkin II: a Fortran chemical kinetics package for the analysis of gas-phase chemical kinetics, Report No. SAND89-8009B, Sandia National Laboratories, USA, 1996.
- [37] M.E. Coltrin, R.J. Kee, F.M. Rupley, Surface Chemkin: A Fortran package for analyzing heterogeneous chemical kinetics at the solid surface-gas phase interface, Report No. SAND90-8003C, Sandia National Laboratories, USA, 1996.
- [38] R.J. Kee, G. Dixon-Lewis, J. Warnatz, M.E. Coltrin, J.A. Miller, A Fortran computer code package for the evaluation of gas-phase multicomponent transport properties, Report No. SAND86-8246, Sandia National Laboratories, USA, 1996.
- [39] H.K. Moffat, R.J. Kee, J.F. Grcar, J.A. Miller, Surface P.S.R.: A Fortran program for modeling well-stirred reactors with gas and surface reactions, Report No. SAND91-8001, Sandia National Laboratories, USA, 1993.
- [40] R. Sui, J. Mantzaras, E. Es-sebbar, M.A. Safi, R. Bombach, Impact of gaseous chemistry in H₂-O₂-N₂ combustion over platinum at fuel-lean stoichiometries and pressures of 1.0–3.5 bar, Energy Fuels 31 (2017) 11448–11459.